

# Android GNSS Measurements under Spoofing and Interference

Andrea Botticella<sup>\*†</sup>  
andrea.botticella@studenti.polito.it

Renato Mignone<sup>\*†</sup>  
renato.mignone@studenti.polito.it

Elia Innocenti<sup>\*†</sup>  
elia.innocenti@studenti.polito.it

Simone Romano<sup>\*†</sup>  
simone.romano2@studenti.polito.it

## ABSTRACT

This study explores the behavior of GNSS navigation on a commercial Android smartphone by analyzing raw measurements collected in both static and dynamic conditions. Using Google’s GNSS Logger and MATLAB-based post-processing, we evaluate PVT (Position, Velocity and Time), signal quality, and clock stability under normal operation and under spoofed inputs—where false positions and delays are injected into the data. The results highlight the vulnerability of smartphone GNSS to software spoofing and underline features that may aid in anomaly detection.

## 1 INTRODUCTION

Global Navigation Satellite Systems (GNSS) are fundamental to modern positioning services, widely embedded in smartphones and critical infrastructure. Despite their ubiquity, GNSS signals are inherently vulnerable to **spoofing**—an attack technique where counterfeit signals deceive the receiver into computing false location or timing information. To develop robust mitigation strategies, it is essential to understand how smartphone GNSS systems behave under both normal and manipulated conditions.

This work investigates the GNSS measurement behavior of a consumer-grade **Android smartphone** across different operating scenarios. We analyze baseline performance by collecting and processing raw GNSS data in two real-world environments: a static session on viewpoint of *Monte dei Cappuccini* and a dynamic session aboard a tram in urban *Turin*. In addition to this baseline study, we simulate spoofing by injecting false position inputs into the processing pipeline and, separately, by introducing artificial delays. The remainder of this report is organized as follows.

- **Section 2** describes the experimental setup, including device configuration, data collection procedures, and the processing pipeline.
- **Section 3** presents results and discussion, contrasting static versus dynamic performance, examining spoofed-location impacts, and analyzing delay effects.
- **Section 4** summarizes the key findings and outlines directions for future work.

## 2 METHODS

### 2.1 Devices and Software

We used a Samsung Galaxy A51 with Android 13 for this experiment. GNSS Logger v3.1.0.4 [8] was chosen due to its unrestricted

access to raw GNSS measurements, compatibility with newer Android APIs, and ability to record detailed GNSS data that is suitable for precise analysis. MATLAB R2024b [10] was employed to handle data because it comes with Google’s GNSS toolbox [7], which accommodates robust analysis and visualization of GNSS measurements and position solutions.

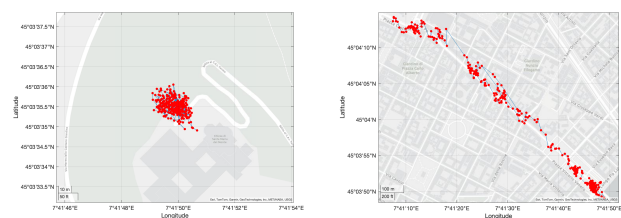
### 2.2 Data Collection Procedure

Two distinct 5-minute GNSS data logging sessions were conducted on 3 May 2025, under cloudy weather conditions, using the GNSS Logger app configured with the following settings enabled:

- **GNSS Location:** to capture location data.
- **GNSS Measurements:** to log raw GNSS measurements.
- **Navigation Messages:** to capture navigation data.
- **GnssStatus:** to log GNSS status information.
- **Sensors:** to capture sensor data.

The sessions were designed to capture both static and dynamic GNSS performance, with the following details:

- Static Scenario:** performed on the viewpoint of *Monte dei Cappuccini, Turin*, starting at 10:35:20. The device was stationary throughout the entire session, providing baseline measurements.
- Dynamic Scenario:** conducted on tram line 15 from *Piazza Castello* to *Piazza Vittorio Veneto*, starting at 10:00:21, simulating a typical urban mobility scenario.



(a) Monte dei Cappuccini.

(b) Tram Line 15.

Figure 1: Comparison of GNSS data: static (a) and dynamic (b) scenarios.

### 2.3 Processing Pipeline

The raw GNSS data from the GNSS Logger served as the input dataset for MATLAB. Processing involved a scripted workflow via `ProcessGnssMeasScript.m` [12], where the following steps were executed:

1. **Filtering:** data points not meeting predefined quality thresholds, such as signal strength or satellite geometry, were excluded to improve accuracy.

<sup>\*</sup>The authors collaborated closely in developing this project.

<sup>†</sup>All the authors are students at Politecnico di Torino, Turin, Italy.

2. **Measurement Extraction:** pseudorange and Doppler measurements were computed from GNSS timestamps and satellite transmission data.
3. **Weighted Least Squares (WLS) Positioning:** applied to derive precise positioning and clock bias estimates.
4. **Visualization and Comparison:** output plots from MATLAB, including pseudorange, pseudorange rates, and position solutions, were generated to facilitate comparative analysis of the static and dynamic scenarios.

## 2.4 Spoofed-Input Configuration

Spoofing scenarios were emulated by introducing artificial variations to the recorded GNSS data through MATLAB processing. Specifically, mock positions were assigned by adjusting the parameter `spoof.position`, which represents modified latitude, longitude, and altitude coordinates. Additionally, artificial time delays were tested by adjusting the `spoof.delay` parameter, typically in milliseconds, to mimic delayed GNSS signal arrival, and `cfg.t_start` parameter to make the spoofed signal appear some seconds after the start of the session. Such configurations facilitated evaluation of the impact of spoofing scenarios on position estimation reliability and accuracy.

## 2.5 Interference Scenario

The experimental setup involved enclosing a smartphone within three layers of aluminum foil while simultaneously exposing it to nearby sources of electromagnetic interference, including two active smartphones engaged in a call and multiple Bluetooth-enabled devices. This configuration created a non-ideal environment for GNSS signal reception. The aluminum enclosure acted as a rudimentary Faraday cage, partially obstructing direct line-of-sight between the device's antenna and GNSS satellites, thereby weakening incoming signals. Concurrently, the proximity of active communication devices introduced broadband RF interference, likely overlapping with GNSS frequency bands and degrading signal quality further.

# 3 RESULTS AND DISCUSSIONS

## 3.1 Baseline Performance: Static vs. Dynamic

Comparing the static and dynamic scenarios highlights key differences in GNSS signal behavior, measurement stability, and receiver performance. Although both datasets were collected under similar atmospheric conditions, the receiver's motion in the dynamic case introduced visible changes across all GNSS indicators.

### Pseudoranges vs Time.

The pseudorange measurements reveal distinct trends across scenarios. In Fig. 2a **more satellites** (e.g., SVs 27, 4, 20, 5, 16, 28, 29, 18) are consistently tracked, exhibiting **flat trajectories** with minimal variation (range:  $\sim 2.1\text{--}2.5 \times 10^7$  m). This suggests stable signal acquisition under favorable conditions. In contrast, Fig. 2b displays **fewer visible satellites** (e.g., SVs 28, 29, 31, 12, 18), with several signals showing abrupt shifts or non-linear behavior (range:  $\sim 2.0\text{--}2.6 \times 10^7$  m). The reduced satellite count in Plot B implies **challenging signal reception**, possibly due to environmental interference or motion-induced signal degradation.

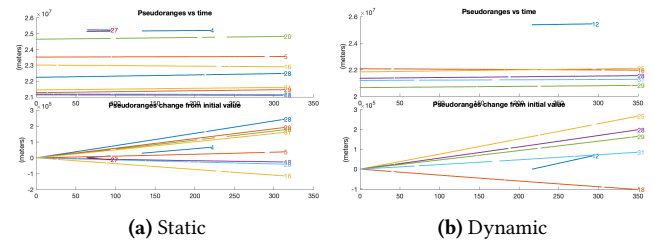


Figure 2: Comparison of Pseudoranges vs Time

### Pseudorange Change from Initial Value.

Deviations from initial values further highlight differences. In Fig. 2a, all tracked satellites follow **shallow linear trends** ( $\pm 0.5\text{--}2$  m), reflecting predictable signal dynamics. The consistency across satellites (e.g., SVs 27, 28, 29) suggests robust tracking of both strong and weaker signals, including those from higher-elevation satellites. Conversely, Fig. 2b shows **steeper slopes** (up to  $\pm 3$  m) and fragmented trends, with notable examples like SV 12 (sudden jump after  $\sim 200$  s) and SV 18 (continuous negative drift). The variability in Plot B indicates **intermittent signal loss or multipath effects**, particularly for satellites with marginal signal strength.

### Positioning and Speed.

In the plots depict positional estimates. Fig. 3a displays a clustered distribution around its median ( $45.059862^\circ, 7.697191^\circ$ ), with a 50% confidence ellipse spanning  $\sim \pm 15$  m. This indicates stable positioning with minimal drift. In contrast, Fig. 3b shows a widely scattered pattern centered at ( $45.066832^\circ, 7.692336^\circ$ ), featuring a 50% ellipse extending  $\sim \pm 400$  m. The median in Plot B lacks practical relevance due to extreme positional variability, unlike Plot A's median, which accurately represents stationary behavior.

The middle plots highlight horizontal speed trends. Fig. 3a exhibits near-zero speeds ( $< 2$  m/s) with minor oscillations, consistent with negligible movement. Conversely, Fig. 3b reveals erratic fluctuations, including a peak exceeding 20 m/s.

The bottom plots compare HDOP and satellite visibility. Fig. 3a maintains low HDOP ( $< 5$ ) with consistent visibility of 8-10 satellites, reflecting robust signal geometry. In contrast, Fig. 3b shows elevated HDOP (up to  $\sim 10$ ) alongside reduced satellite counts (4-6), indicating degraded tracking conditions.

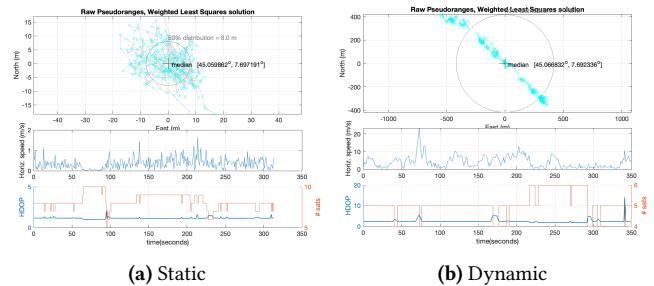


Figure 3: Comparison of Position, Speed, and HDOP

### State Offsets and Timing Bias.

The **top plots** illustrate position state offsets relative to the median. In Fig. 4a, deviations in latitude, longitude, and altitude remain tightly constrained within  $\sim \pm 50$  m, with smooth, gradual fluctuations indicating stable signal tracking. In contrast, Fig. 4b exhibits

extreme offsets exceeding  $\pm 500$  m, punctuated by abrupt spikes (e.g., a  $\sim 600$  m jump near 150 seconds). The **second plot** shows clock bias (common bias) trends. Both plots exhibit linear growth, but in Fig. 4a increases steadily ( $\sim 200$  ns over 350 seconds), reflecting predictable receiver clock drift. Fig. 4b escalates more sharply ( $\sim 250$  ns over the same interval), with a notable dip aligning with the positional spike in the top plot. This correlation implies transient disruptions affecting both position and timing stability in Plot B. Velocity state estimates (**third plot**) further differentiate the two scenarios. Fig. 4a shows near-zero velocities (all components  $\leq 2$  m/s), consistent with negligible movement. Fig. 4b, however, displays pronounced oscillations, particularly in the northward direction (peaks  $\pm 20$  m/s), indicating rapid or inconsistent motion. The **bottom plots** depict common frequency offset trends. Fig. 4a maintains a stable trajectory near 0.8 ppm, with minor perturbations. Fig. 4b shows greater variability, including a sharp downward deviation during the positional spike. This suggests that signal degradation or motion-induced errors propagate to both position and frequency estimates in Plot B, unlike the consistent behavior seen in Plot A.

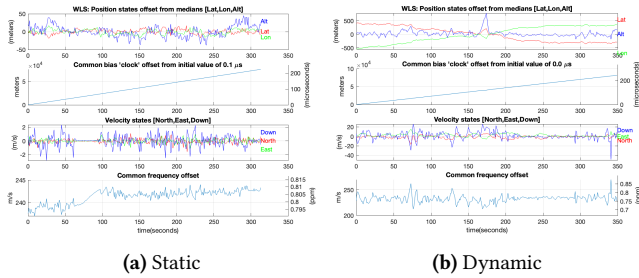


Figure 4: Comparison of WLS states and bias

These measurements highlight the importance of scenario-aware processing: identical hardware, firmware, and atmospheric conditions can yield centimetre-per-second stability on a quiet terrace, yet the very same setup will produce hundred-metre excursions once placed on a moving tram through an urban canyon.

### 3.2 Impact of Spoofed Position

In a spoofing attack, counterfeit signals are broadcast to mimic GNSS transmissions, often altering their timing, amplitude, or content. Typically, these deceptive signals are sent at higher power than the originals to mislead navigation systems. In our experiment, however, spoofing was implemented purely in software by adjusting the perceived reception time inside the professor’s script to simulate spoofing behavior.

For the spoofed test we manually injected the coordinates of **Piazza Vittorio Veneto** (45.064749, 7.695466) — a location adjacent to our true survey point — directly into the processing script. As shown in the plots, this causes the solver to converge exactly at the Piazza Vittorio Veneto coordinates rather than the true measurement site, introducing a horizontal displacement of several hundred metres. Despite this spatial shift, all raw observables remain essentially unchanged relative to the normal run:

- **Carrier-to-noise density (C/N):** The plot of the signal quality remains unchanged compared to the base case, this because the

signals are just replayed with a different timing to the victim. **Pseudorange residuals:** The overall spread remains the same, but the entire residual distribution is offset by the constant delay corresponding to the spoofed displacement.

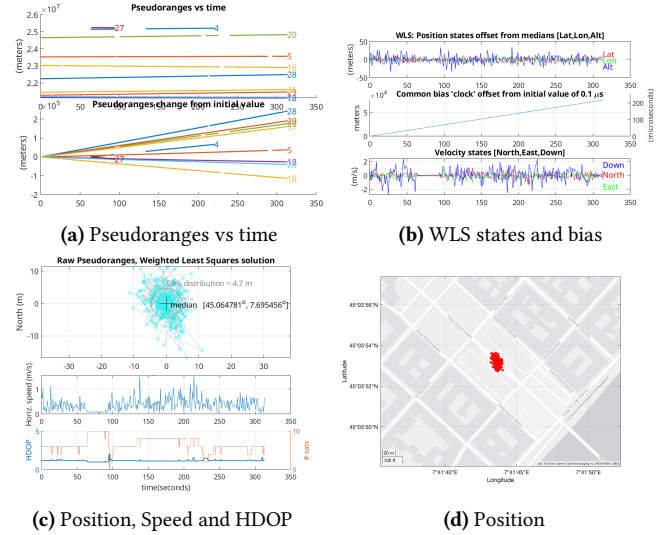


Figure 5: Spoofing scenario plots

Additionally, the 50% (interquartile) range in the median-error distribution shrinks from approximately 8 m in the genuine case to about 4.7 m under spoofing. This reduction occurs because the solver consistently “locks” onto the spoofed coordinate, decreasing variability around that false point.

### 3.3 Effects of Timing Delays

In this delayed-spoofing scenario we again target the same true survey point but now introduce a software-only replay delay: the spoofer “listens” to genuine signals, waits 1 ms, then injects the spoofed Piazza Vittorio Veneto coordinates starting at 50 s into the run. Key parameters: `cfg.delay = 1e-3`; `cfg.t_start = 50`. As visible in the plots, all observables remain nominal until  $t=50$  s, at which point the solver’s estimated position and receiver clock-bias exhibit a clear discontinuity as the spoof takes effect.

- **Position solution:** Prior to 50 s, the estimated coordinate coincides with the true static point. Immediately after 50 s, the solution jumps to the spoofed Piazza Vittorio Veneto location, replicating the static-spoof offset of several hundred metres.
- **Receiver clock-bias:** A sudden step of appears in the estimated receiver clock-bias track, directly corresponding to the 1 ms replay delay needed to shift the range solution by the planar offset.
- **Carrier-to-noise density (C/N):** The C/N time-series shows no amplitude change at  $t=50$  s—signal strength is unaffected by delay.
- **Pseudorange residuals:** Residuals maintain the same spread, but their mean shifts abruptly at 50 s by the additional delay  $\delta t$ .

Even a 1 ms replay delay can therefore introduce a large positional error and matching clock-bias shift without altering any standard

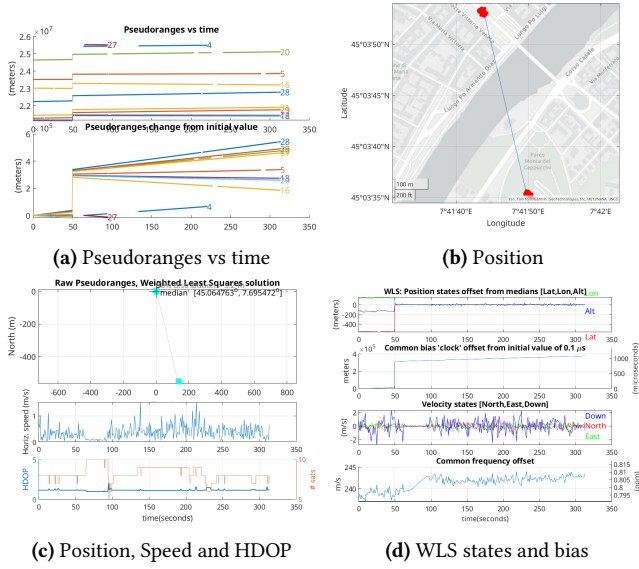


Figure 6: Spoofing plus Delay scenario plots

observables. Detecting such covert delay-based spoofing thus requires monitoring for timing discontinuities.

### 3.4 Interference Effects

Analyzing the logged data reveals several hallmark effects of this compromised environment. A key detail is that **data collection began before the foil shielding was applied**. During this initial phase, the receiver operated under normal conditions and successfully acquired a large number of satellites with strong signals. However, once the shielding was added, the number of tracked satellites dropped significantly, and signal quality degraded—clear in the plots by a drop in C/N values and clock discontinuities.

Pseudorange measurements (Figure 7a), which estimate the distance between the receiver and satellites, exhibit gradual drift over time, indicative of accumulating errors due to signal instability. The carrier-to-noise density ( $C/N_0$ ) metric (Figure 7b) shows **sharp initial drops followed by slow recovery**, reflecting the receiver's struggle to reacquire and track satellite signals through the combined effects of shielding and interference. Velocity estimates derived from Doppler shifts display erratic fluctuations, particularly during periods of heightened interference, suggesting corrupted phase measurements. Position solutions (Figure 7d) computed via weighted least squares exhibit significant horizontal and vertical deviations from expected values, with error distributions expanding over time as the receiver compensates for inconsistent pseudorange inputs.

In such scenario, the interplay between physical obstructions and electromagnetic noise creates a hostile operating environment for GNSS receivers. The aluminum enclosure not only attenuates signal power but also shields the signals. Nearby devices, meanwhile, introduce spurious signals that desensitize the receiver's front-end, increasing the likelihood of cycle slips (loss of phase lock) and pseudorange outliers. These findings reinforce the **sensitivity of GNSS systems to real-world complexities**, where idealized assumptions of unobstructed, interference-free signal propagation rarely

hold. Practical applications in urban canyons, dense foliage, or near industrial RF emitters may thus encounter similar challenges, necessitating robust mitigation strategies.



Figure 7: Interference effects on GNSS measurements

## 4 CONCLUSIONS

This research compared GNSS performance on a commercial smartphone under static, dynamic, and spoofed scenarios based on raw measurements and post-processing in MATLAB. Under the static scenario, the device had consistent position estimates, low clock drift, and negligible variation in pseudorange and speed. The dynamic scenario, on the other hand, demonstrated higher noise in position, pseudorange rates, and clock bias—predictable effects of motion and satellite geometry variations. The spoofing tests indicated that even basic, software-level injection in the form of taking on false coordinates by the GNSS solver, as it settles on a consistent but incorrect position with little or no impact on first-order signal measurements like carrier-to-noise ratio or HDOP. This highlights a significant vulnerability: smartphone GNSS receivers can be fooled without revealing obvious degradations in signal quality.



## A APPENDIX

### A.1 GNSS Logger Screenshots

The following figures show screenshots from the GNSS Logger app, illustrating various features and data visualizations available during the GNSS data collection process of the *Monte dei Cappuccini* test.

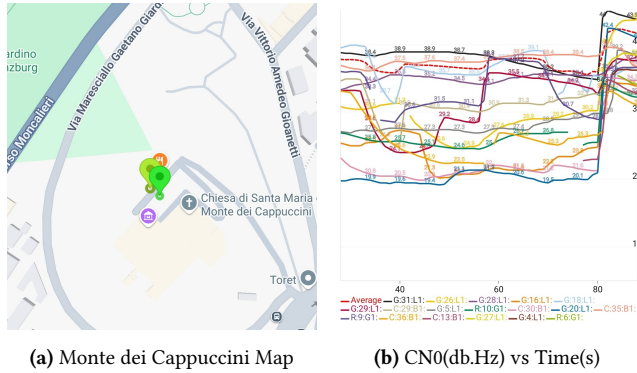


Figure 8: GNSS Logger Map (a) and Plots (b).

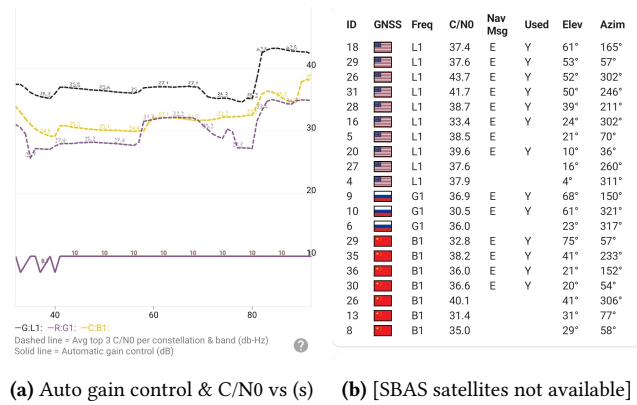


Figure 9: GNSS Logger Spoof/Jam (a) and Status (b).

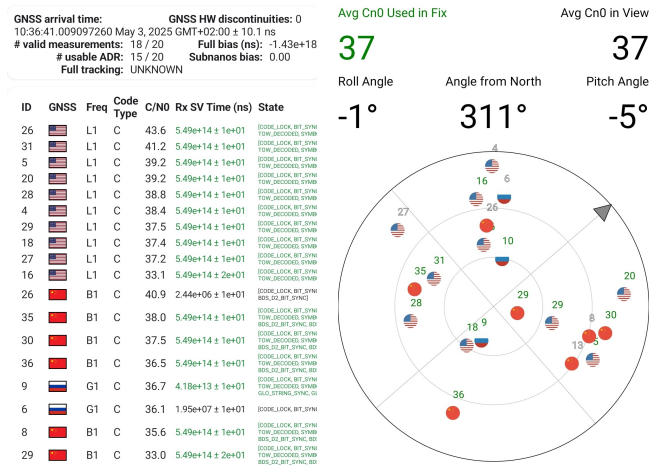


Figure 10: GNSS Logger Measurements (a) and Skyplot (b).

## REFERENCES

- [1] 2025. GNSS Planning. Web application. (2025). <https://www.gnssplanning.com/#/settings>
- [2] 2025. LatLongData. Web application. (2025). <https://www.latlongdata.com/elevation/>
- [3] Android Developers. 2025. GnsMeasurement. Android SDK reference. (2025). <https://developer.android.com/reference/android/location/GnsMeasurement>
- [4] Simon Banville and Frank van Diggelen. 2016. Precise GNSS for Everyone: Precise Positioning Using Raw GPS Measurements from Android Smartphones. *GPS World* 27, 11 (November 2016). <http://gpsworld.com/innovation-precise-positioning-using-raw-gps-measurements-from-android-smartphones/>
- [5] Alan Cameron. 2016. Google opens up GNSS pseudoranges. *GPS World* (7 June 2016). <https://www.gpsworld.com/google-opens-up-gnss-pseudoranges/>
- [6] European GNSS Agency (GSA). 2018. *Using GNSS Raw Measurements on Android Devices: Towards better location performance in mass market applications*. Technical Report. GSA GNSS Raw Measurements Task Force. <https://galileognss.eu/wp-content/uploads/2018/05/Using-GNSS-Raw-Measurements-on-Android-devices.pdf>
- [7] Google LLC. 2025. GNSS Analysis Tools v2.0.0.1. GitHub release. (2025). <https://github.com/google/gps-measurement-tools/releases/tag/2.0.0.1>
- [8] Google LLC. 2025. GNSS Logger v3.1.0.4. Android app on Google Play. (2025). <https://play.google.com/store/apps/details?id=com.google.android.apps.gnsslogger>
- [9] Google LLC. 2025. Google Maps. Web application. (2025). <https://www.google.com/maps>
- [10] The MathWorks, Inc. 2024. *MATLAB R2024b*. Natick, Massachusetts, United States. <https://www.mathworks.com/products/matlab.html>
- [11] Frank van Diggelen. 2018. GNSS Measurements Update. In *GSA Raw Measurements Workshop*. Prague, Czech Republic. [https://www.gsa.europa.eu/sites/default/files/expo/frank\\_van\\_diggelen\\_keynote\\_android\\_gnss\\_measurements\\_update.pdf](https://www.gsa.europa.eu/sites/default/files/expo/frank_van_diggelen_keynote_android_gnss_measurements_update.pdf)
- [12] WDCSecure. 2025. LabGNSS: material and documentation for the GNSS Lab. GitHub repository. (2025). <https://github.com/WDCSecure/LabGNSS.git>